Engineered Science
DOI: https://dx.doi.org/10.30919/es1571

Enhancement of the Biological Activity of Catechin from *Uncaria gambir* as Anticancer Agents through Molecular Encapsulation Studies: Experimental and Computational Approaches

Nanik Siti Aminah,[1,2,*] Muhammad Ikhlas Abdjan,[3] Abdullahi Musa,[1] Muggundha Raoov s/o Ramachandran,[4] Faizah Binti Mohammad Yunus,[4] Nozlena Abdul Samad,[5] Alfinda Novi Kristanti,[1,2] Tin Myo Thant,[6] Imam Siswanto[1] and Rico Ramadhan[1]

Abstract

Catechin, a bioactive flavonoid derived from Uncaria gambir, exhibits significant anticancer potential but is limited by its poor aqueous solubility and low bioavailability. To overcome these challenges, this study investigates the molecular encapsulation of catechin with β-cyclodextrin (βCD) and hydroxypropyl-β-cyclodextrin (HPβCD) through experimental and computational approaches. Structural characterisation using field emission scanning electron microscopy (FESEM), X-ray diffraction (XRD) and nuclear magnetic resonance (NMR) spectroscopy confirmed the successful formation of inclusion complexes, with HPβCD exhibiting superior amorphisation and molecular dispersion, suggesting enhanced solubility. Additionally, in silico molecular studies through molecular docking and molecular dynamics simulations of the inclusion complexes were conducted. The results demonstrate no significant change in the coordinates of catechin inside the cavities of both materials. In particular, the Cat-HPβCD complex exhibited stronger binding free energy (ΔGbind) through several end-point free energy approaches estimated in this research. Furthermore, Cat-HPβCD complex shows a significant cytotoxic effect against MCF-7 breast cancer cells time-dependent, achieving IC50 values of 14 µg/mL and 10 µg/mL at 48 and 72 hours, respectively. These findings highlight HPβCD as an optimal carrier for catechin, enhancing its solubility, stability, and anticancer efficacy, paving the way for its potential pharmaceutical applications.

Keywords: Catechin; β-cyclodextrin; Inclusion complex; Molecular studies; Breast cancer.
Received: 24 March 2025; Revised: 21 May 2025; Accepted: 07 June 2025.
Article type: Research article.

1. Introduction

Indonesia is the leading global exporter of gambier, supplying approximately 80% of the international market demand. Most production occurs in West Sumatra, with an estimated output of 2,491.39 tons recorded in 2018.[1] This production is predominantly carried out on a small scale by local farmers. Gambier is obtained as a hot-water extract from the leaves and twigs of the gambier plant (*Uncaria gambir* (Hunter) Roxb.). Traditionally, the extract is chewed as a herb and consumed for its antidiarrheal and antioxidant properties.[2,3] The hooks of *Uncaria gambir* are conventionally prepared for the treatment of wounds, ulcers, fever, asthma, rheumatism, hyperpyrexia, hypertension, headaches, gastrointestinal illness, and bacterial or fungal infections.[4] Several of these conditions are associated with chronic inflammation and oxidative stress, mechanisms that also underpin cancer development. Thus, traditional use implies potential for anticancer activity, particularly due to its rich polyphenolic content.[5,6] Chemically, gambier is composed of 7.63–23.16% water, 12.24–24.16% tannins, 14.76–86.71% catechins, 1.43–25.24% ash, and 5.58–46.28% water-insoluble compounds.[7,8] Since catechin is the most abundant component in gambir, isolating it could significantly enhance the value and export potential of this product (Fig. 1a).

The development of treatment methods for degenerative

[1] *Department of Chemistry, Faculty of Science and Technology, Universitas Airlangga, Komplek Kampus C UNAIR, Jl. Mulyorejo, Surabaya, 60115, Indonesia*

[2] *Biotechnology of Tropical Medicinal Plants Research Group, Universitas Airlangga, Komplek Kampus C UNAIR, Jl. Mulyorejo, Surabaya, 60115, Indonesia*

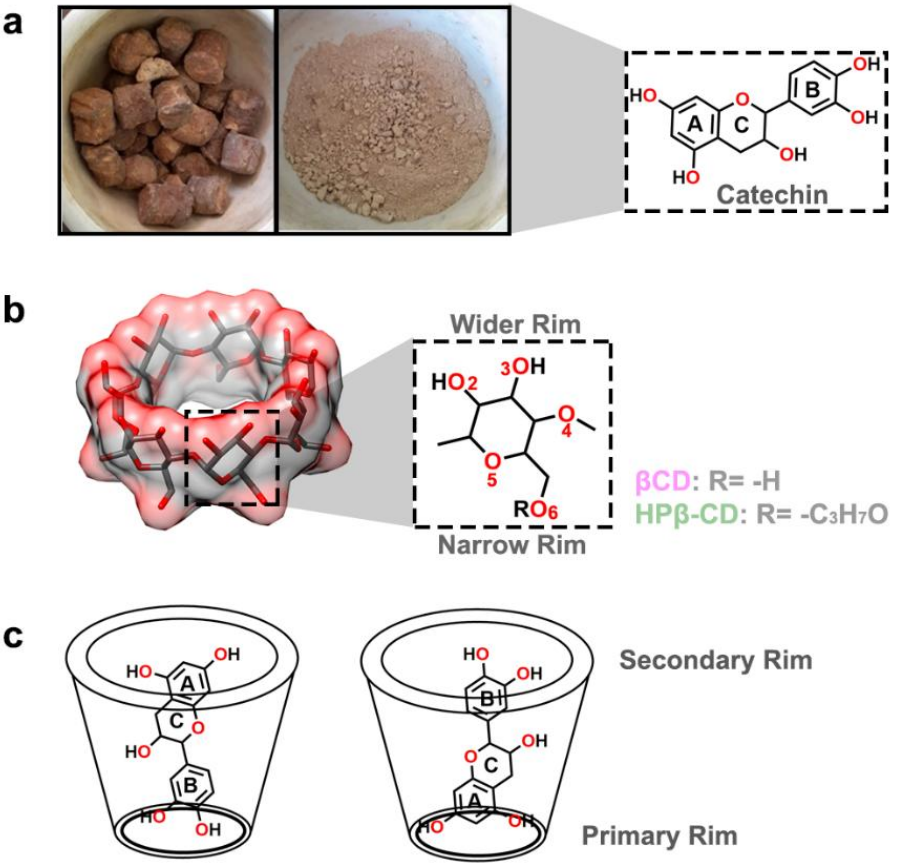

Fig. 1: (a) The isolated Catechin (Cat) from sap *Uncaria gambir*, (b) cyclodextrin structure as host material (βCD and HPβCD), and (c) the possibility conformation of catechin inside the cavity of host material.

diseases, such as cancer, remains a significant challenge today. Data from the WHO Global Cancer Observatory 2022 indicates that Cervical cancer is the fourth most common cancer in women globally with around 660,000 new cases and around 350 000 deaths worldwide.[9] Current cancer treatments primarily rely on chemotherapy methods, which often have side effects on the body.[10] In light of these limitations, exploring drug preparations from natural ingredients presents a promising opportunity due to their abundant availability and safety profile.[11] However, some drug compounds derived from natural ingredients do not work as effectively against cancer cells compared to synthetic compounds. Therefore, modifying the physicochemical properties of natural compounds is necessary to enhance their biological activity as anticancer agents.

Catechin (Cat), a polyphenolic compound, are effective scavengers of reactive oxygen species, and their antioxidant properties are of great interest in dietetics and cosmetology.[12] They have been reported to enhance mental and behavioral symptoms of dementia, including dementia with lewy bodies and aggressiveness in patients with Alzheimer's disease.[13] Furthermore, their antiviral and cancer-inhibiting properties could have pharmaceutical applications.[14] However, catechin powders are poorly soluble in water and easily oxidized.[15] Consequently, the potential for catechins to reach the target proteins responsible for cancer cell development is suboptimal. Therefore, improving solubility is essential to enhance the potential of catechins as anticancer agents. On the other hand, cyclodextrins (Fig. 1b) are a type of truncated-cone polysaccharide mainly composed of six to eight D-glucose monomers linked by α-1,4-glucose bonds with a hydrophobic central cavity and a hydrophilic outer surface, which allow them to encapsulate model substrates and form host-guest complexes or supramolecular species (Fig. 1c). This capability enhances the drug solubility in aqueous solutions and affects the chemical characterization of drugs.

Several studies have explored catechin encapsulation with βCD or its derivatives to improve antioxidant delivery or shelf-life. For instance, Chagam *et al.* (2020) reported enhanced physicochemical properties, thermal stability, and

[3] *Department of Chemistry, Faculty of Mathematics and Natural Science, Universitas Negeri Surabaya, Surabaya, 60213, Indonesia*

[4] *Departmen of Chemistry, Faculty of Science, University of Malaya, Kuala Lumpur, 505603, Malaysia*

[5] *Department of Toxicology, Advanced Medical and Dental Institute, Universiti Sains Malaysia, Kepala Batas, Penang, 13200, Malaysia*

[6] *Department of Chemistry, Mandalay University, Mandalay, 05032, Myanmar*

* *E-mail:* nanik-s-a@fst.unair.ac.id (S. A. Nanik)

antioxidant activity of catechins through inclusion complexation with β-cyclodextrin.[16] Similarly, Zhang *et al.* (2025) demonstrated that hyperbranched cyclodextrin–catechin inclusion complexes exhibited improved stability, antioxidant, and antimicrobial properties.[17] However, limited studies have focused specifically on enhancing anticancer activity via such inclusion complexes, and even fewer have combined both experimental and computational approaches. In our previous research, we reported the anticancer activity of Nano *Uncaria gambir*.[18] Building on this, the present study involves the isolation and characterization of catechin from *Uncaria gambir*. Furthermore, to improve the absolute bioavailability of catechin towards cervical cancer, we investigated its interaction with a series of cyclodextrins, including β-Cyclodextrin (βCD) and 2-hydroxypropyl-β-cyclodextrin (HPβCD). We observed various factors that affect complexation selectivity and stabilization. Additionally, we conducted molecular modeling studies to build three-dimensional models of βCD and HPβCD upon complexation with catechin to provide a more detailed description of the interactions, thereby rationalizing the experimental results. Finally, we studied the anticancer potential of both catechin and its encapsulated derivatives against breast cancer (MCF-7) cell lines (Fig. 2).

2. Experimental section

2.1 General

The *U. gambir* sap was obtained from traditional markets in Surabaya, Indonesia. The plant material was authenticated and assigned a voucher specimen (No. 547/02.Genbinesia/2023) at Yayasan Generation Biology Indonesia. β-cyclodextrin (βCD) and 2-hydroxypropyl-βcyclodextrin (HPβCD) were purchased from Sigma–Aldrich Inc. St. Louis, MO. UV-Vis measurement was conducted using UV-1800, respectively. The X-ray diffraction (XRD) powder diffraction pattern was recorded on an X-ray diffractometer (AXS D8 Advance, Bruker Inc., Germany) using Ni-filtered Cu K α radiation (λ = 1.5406 Å) at a voltage of 40 kV and a current of 40 mA, while the morphology was recorded using a SU-8010 environmental scanning electron microscope system (Hitachi Company, Tokyo, Japan). A 600 MHz Bruker spectrometer was employed to measure the ^{1}H and ^{13}C nuclear magnetic resonance (NMR) spectra in MeOH solutions. The coupling constants and chemical shifts are reported in Hz and ppm, respectively. Silica gel Merck 60 GF254 was used for vacuum liquid chromatography (VLC), while silica gel Merck G60 was used for gravity column chromatography (GCC). Thin layer chromatography (TLC) was performed on an aluminum plate coated with Silica gel Merck Kieselgel 60 GF254. The melting point was determined using a Fisher Johns Melting Point Apparatus.

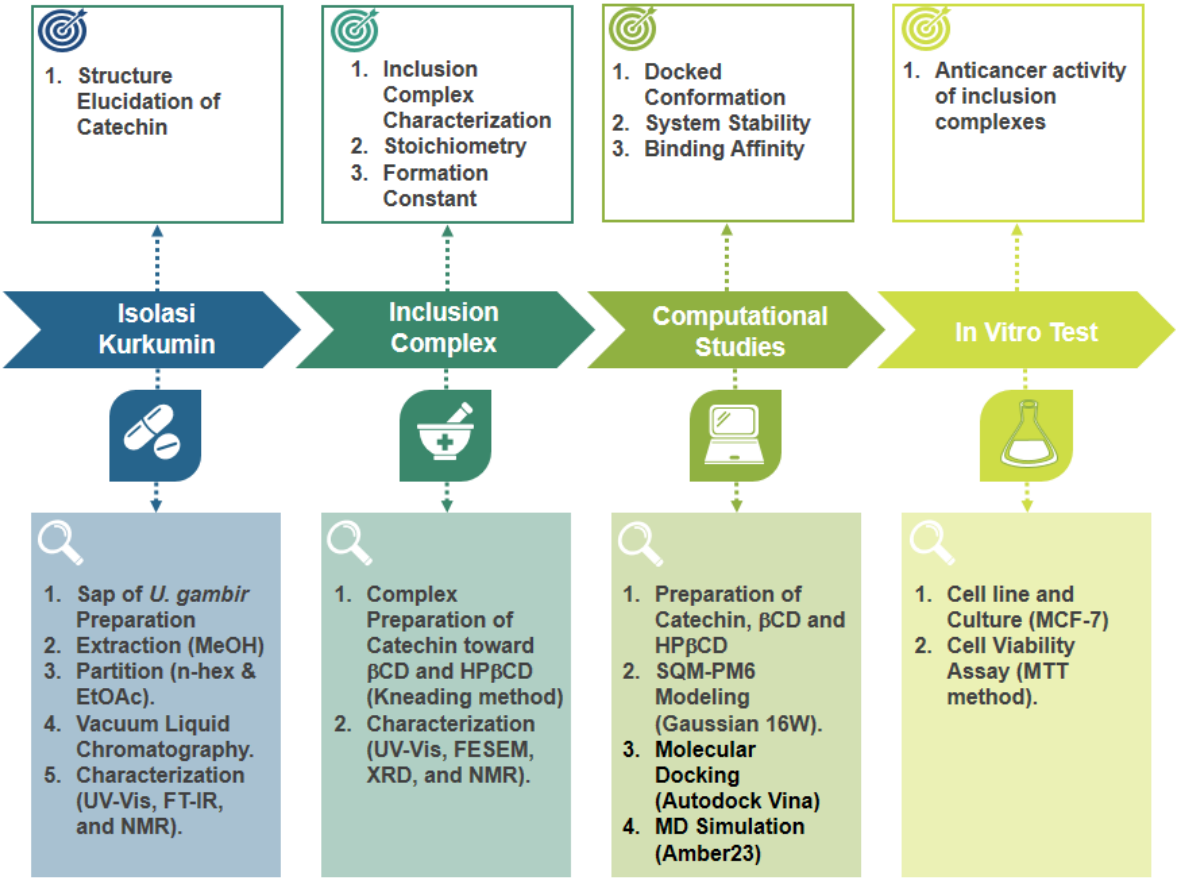

Fig. 2: Schematic diagram of the research.

2.2 Extraction, isolation, and characterization

The dried *U. gambir* sap (500 g) was extracted using maceration with methanol at room temperature for 3 x 24 hours. The resulting methanol extract was concentrated using a rotary vacuum evaporator and partitioned sequentially with n-hexane and ethyl acetate, yielding n-hexane, ethyl acetate, and methanol residue extracts. The ethyl acetate extract (60 g) was evaporated and subjected to vacuum liquid chromatography (VLC) using a dichloromethane and methanol gradient elution system with increasing polarity (100% to 70:30). At eluent system of dichloromethane and methanol (90:10), Catechin, along with some impurities, was obtained. Further purification of catechin was performed using gravity column chromatography (GCC) with a similar dichloromethane-methanol gradient (100% to 80:20). Pure catechin was successfully isolated at the 90:10 elution ratio. The structure of the purified catechin was confirmed through various structural elucidation techniques, including Nuclear Magnetic Resonance (NMR) spectroscopy, UV-Vis, and Fourier Transform Infrared (FTIR) spectroscopy, following a purity assessment.

2.3 Inclusion complex preparation

Catechin-β-cyclodextrin (Cat-βCD) complexes were prepared using the conventional kneading method.[19] Catechin and βCD were mixed in a 1:1 ratio and kneaded for 30 minutes with a minimal amount of water. The 1:1 ratio was selected based on preliminary phase solubility studies (see Section 3.2.2), which indicated the formation of a stable inclusion complex with a 1:1 stoichiometry. The resulting homogeneous paste was collected and dried to constant mass for subsequent analysis. The same procedure was applied for HPβCD. The calculated percentage yields were 76% for βCD and 70% for HPβCD. D_2O was used as the solvent for the ^{1}H-NMR analyses.

2.4 Stoichiometry and formation constant studies

In this study, changes in absorbance intensities were observed when the concentration of the analyte (Cat) was held constant at 0.1 mM, while the concentrations of βCD and HPβCD were increased (0.001, 0.002, 0.003, and 0.004 M).[20] A phase solubility diagram was created by plotting 1/A against 1/[βCD & HPβCD], where A represents the maximum absorbance of catechin and [βCD & HPβCD] denotes the concentration of βCD or HPβCD, respectively. Using this diagram, the stoichiometric ratio and formation constant (K) were determined with the modified Benesi–Hildebrand equation.[21,22] The K value was calculated by dividing the slope with the intercept of the straight line obtained from the double reciprocal plot.

2.5 System preparation

The modeled catechin (Cat) was optimized using the Semi-Empirical Quantum Method-Parametric method 6 (SQM-PM6) through the Gaussian 16W package. This method was selected to calculate the electrostatic potential (ESP) charge.[23] Optimization aims to calculate ESP charge for organic small molecules. Meanwhile, the βCD and HPβCD structures were prepared using the Chimera 1.13 package to calculate several crucial parameters for further analysis, such as force field, bonded, non-bonded, and charge.

2.6 Molecular docking

The prepared Cat, βCD, and HPβCD structures from the previous step are used to perform the inclusion complexation through molecular docking. It was performed by AutoDockTool version 1.5.6 and AutoDock Vina packages. These packages were considered due to their balance of stability, ease of use, and compatibility with established docking protocols. Molecular docking helps determine the initial conformation of small molecules inside the cavity of the host material.[24] The grid box was constructed to cover all surfaces of the host material, with the number of points in the x, y, and z dimensions set to 40 (βCD) and 55 (HPβCD), respectively. Then, docked conformations from the obtained inclusions were selected based on the lowest dock score. This structure will be used for further evaluation through molecular dynamics (MD) simulation as the initial conformation.

2.7 Molecular dynamics simulation

The inclusion complex was obtained from molecular docking to understand their dynamics behavior through the Amber23 and AmberTools24 packages. The topology of each system was prepared through the *tleap* tool.[25] Moreover, the force field parameter was applied to the topology system, including the *antechamber*[26] module with the AM1-BCC method. Meanwhile, βCD and HPβCD force fields were generated through the Glycam-06,[27] and general AMBER force field (GAFF).[28] Water molecules (octahedral TIP3P model) were added to the inclusion complex with a distance of 15 Å to generate a solvated system. Continue, the solvated inclusion complex was minimized using the steepest descent (maxcyc) of 3000 steps and the conjugate gradient (ncyc) of 1500 steps to reduce bad atomic contact in the system. Then, the system was heated gradually at 10.0 K to 298.0 K over 100 ps using a canonical ensemble (NVT). The following step was the system equilibrium for 1000 ps at a constant temperature (298.0 K). The equilibrated system was simulated under periodic boundary conditions (1 atm and 298K) with the isothermal-isobaric ensemble (NPT). The SHAKE algorithm was applied to constrain hydrogen bonds involved in the system. The Particle Mesh Ewald (PME) method was used to calculate charge-charge interactions (Cut-off: 12 Å).[29] The production step was simulated along 350 ns (three replicates) for each system. It aims to produce the trajectory system for evaluation purposes. It should be noted that the simulation was performed using the Graphical Processing Unit of the *PMEMD.cuda* tool.[30]

2.8 Trajectories analysis

The obtained trajectories were used to calculate several

variables, such as system stability and binding free energy. Through *cpptraj*[31] tool was applied to calculate the root-mean-square of displacement (RMSD), radius of gyration (RoG), distance, and hydrogen bond (Hbond). In particular, binding free energy (ΔG_{bind}) was estimated through *MMPBSA.py*.[32] Several approaches were used to estimate ΔG_{bind}, such as the Molecular Mechanics-Poisson Boltzmann Surface Area (MM-PBSA), Molecular Mechanics-Generalized Born Surface Area (MM-GBSA), and Quantum Mechanics/Molecular Mechanics-Generalized Born Surface Area (QM/MM-GBSA). The estimation of ΔG_{bind} consists of enthalpy (ΔH) and entropy change ($-T\Delta S$) (Eqn. 1). The $-T\Delta S$ term was performed using a Normal Mode (NMODE) approximation. Meanwhile, the ΔH term consists of the free energy of the gas (ΔG_{gas}) and solvation (ΔG_{solv}) terms (Eqn. 2). In detail, the ΔG_{gas} is influenced by van der Waals (ΔE_{vdW}) and electrostatic (ΔE_{ele}). Meanwhile, the ΔG_{sol} is influenced by the Poisson Boltzmann/Generalized Born model ($\Delta G_{solv}^{PB/GB}$), and solvent-accessible surface area energy ($\Delta G_{solv}^{nonpolar}$). In particular, the QM/MM-GBSA approach provides additional energy in the form of self-consistent energy (ΔG_{SCF}). The PM6 semi-empirical method was chosen as the level of theory for the quantum mechanical (QM) region, which was assigned to the guest molecule (Cat). The PM6 semi-empirical method was selected for QM/MM-GBSA calculations because it offers a good balance between accuracy and computational efficiency, especially for organic host–guest systems like cyclodextrin complexes. Although more accurate methods like DFT exist, they are too computationally intensive for analyzing thousands of MD snapshots. Therefore, PM6 was selected, ensuring valuable insight into key interaction energetics without excessive computational cost. The molecular mechanics (MM) region, on the other hand, was applied to the host materials (βCD and HPβCD).

$$\Delta G_{bind} = \Delta H - T\Delta S \quad (1)$$

$$\Delta H = \Delta G_{gas} + \Delta G_{solv} \quad (2)$$

2.9 Biological activity

MCF-7 cells were seeded in 96-well plates at a density of 1×10^4 cells per well and allowed to incubate for 24 hours before treatment. Serial dilutions of βCD, HPβCD, Cat, Cat-βCD, and Cat-HPβCD were prepared in Dimethyl Sulfoxide (DMSO) for the treatments. The final concentrations administered for each compound were 200 µg/ml, 100 µg/ml, 50 µg/ml, 25 µg/ml, and 12.5 µg/ml. The cells were exposed to these treatments for 24, 48, and 72 hours. The effects of the compounds on the viability of MCF-7 cells were assessed using the 3-(4,5-dimethylthiazol-2-yl)-2,5-diphenyltetrazolium bromide (MTT) colorimetric assay.[33] A 5 mg/ml MTT solution was prepared by dissolving MTT powder in sterile Phosphate Buffered Saline (PBS). Following the treatment periods, the media was aspirated and replaced with fresh media containing 10% MTT solution. After a 4-hour incubation, the MTT-media solution was removed, and the purple formazan crystals formed were dissolved in 100 µl of DMSO. The optical density was then measured at 570 nm with a reference wavelength of 620 nm using an absorbance reader. To confirm that DMSO did not contribute to cytotoxicity at the concentrations used, control experiments with DMSO alone (at the highest concentration present in the test samples) were conducted. No significant reduction in cell viability was observed, confirming DMSO compatibility with the MTT assay at these levels.

3. Results and discussion

3.1 Structure elucidation of catechin

Compound 1 (10 g) was characterized as a white crystal with a melting point of 236 °C. Its structure was elucidated through various spectroscopic analyses, such as UV Vis, FTIR, ^{1}H-NMR, ^{13}C-NMR, and 2D techniques including COSY, HSQC, and HMBC (Figs. S1-S11). The UV-Vis (MeOH) spectrum shows λmax (nm) at 281, while the FTIR spectra revealed OH bands at 3276 cm^{-1} (associated with the OH group of phenol), other characteristic bands reveal include 2932 cm^{-1} (indicating C-H stretching) as well as 1622 cm^{-1} (corresponding to C=C stretching). ^{1}H-NMR (600 MHz, MeOD) δ 6.89 [1H, d, J = 2.0 Hz, (H-2')], 6.81 [1H , d, J = 8.1 Hz, (H-5')], 6.77 [1H , dd, J = 8.2, 2.0 Hz, (H-6')], 5.98 [1H, d, J = 2.3 Hz, (H-6)], 5.91 [1H, d, J = 2.3 Hz, (H-8)], 4.62 [1H, d, J = 7.5 Hz, (H-2)], 4.02 [1H, td, J = 7.9, 5.4 Hz, (H-3)], 2.90 [1H, dd, J = 16.1, 5.4 Hz, (H-4A), 2.56 [1H, dd, J = 16.1, 8.1 Hz, (H-4B)]. ^{13}C NMR (151 MHz, MeOD) δ 157.82 (C-7); 157.56 (C-5); 156.90 (C-9); 146.23 (C-3'); 147.21 (C-4'); 132.22 (C-1'); 120.02 (C-6'); 116.07 (C-5'); 115.25 (C-2'); 100.82 (C-10); 96.30 (C-6); 95.51 (C-8); 82.64 (C-2); 69.29 (C-3); 28.49 (C-4).

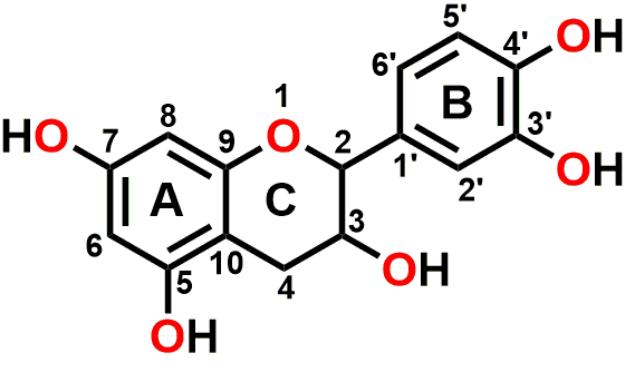

Fig 3: Structure of Isolated Compound (Catechin).

The ^{1}H-NMR analysis indicated the presence of nine protons, with the aromatic protons exhibiting signals at δH 5.98 ppm (H6, d, J = 2.3 Hz), δH 5.91 ppm (H8, dd, J = 2.3 Hz), δH 6.90 ppm (H2', d, J = 2.1 Hz), δH 6.80 ppm (H5', d, J = 6 Hz), and δH 6.77 ppm (H6', dd, J = 6 Hz, and J = 2.1 Hz). Based on the coupling constant values, the H6', H5', and H2' protons formed an ABX system on ring B, while H6 was

Table 1: NMR data (600 MHz, MeOD) of Catechin.

Position	Compound 2 (600 MHz, MeOD)		Ref. [34] (600 MHz, $CDCL_3$)	
	δC (ppm)	δH (ppm) (mult, J in Hz)	δC (ppm)	δH (ppm) (mult, J in Hz)
2	82.6 (CH)	4.62 (d, *J* = 7.5 Hz)	82.6 (CH)	4.56, d
3	69.2 (CH)	4.02 (td, *J* = 7.9, 5.4 Hz	68.3 (CH)	4.06, m
4	28.4 (CH_2)	2.56 (dd, *J* = 16.1, 8.1 Hz)	28.80 (CH_2)	2.53, dd
		2.90 (dd, *J* = 16.1, 5.4 Hz)		2.98, dd
10	100.8 (C)	-	100.6 (C)	-
5	157.5 (C)	-	157.2 (C)	-
6	96.3 (CH)	5.98 (d, *J* = 2.3 Hz)	96.1 (CH)	6.02 (d, j = 2.3 Hz)
7	157.8 (C)	-	157.7 (C)	-
8	95.5 (CH)	5.91 (d, *J* = 2.3 Hz)	95.4 (CH)	5.88 (dd, j = 2.3 Hz)
9	156.9 (C)	-	156.65 (C)	-
1’	132.1 (C)	-	132.1 (C)	-
2’	115.2 (CH)	6.89 (d, *J* = 2.0 Hz)	115.2 (CH)	6.90 (d, j = 2.1 Hz)
3’	146.2 (C)	-	145.6 (C)	-
4’	147.2 (C)	-	147.7 (C)	-
5’	116.0 (CH)	6.81 (d, *J* = 8.1 Hz)	115.6 (CH)	6.80 (d, j = 6 Hz)
6’	120.0 (CH)	6.77 (dd, *J* = 8.2, 2.0 Hz	119.9 (CH)	6.76 (dd, j = 6.0 & 2.1 Hz)

positioned meta to H8 on ring A. The non-aromatic cyclic protons appeared as a doublet at δH 4.62 ppm (H2, d) and as a multiplet at δH 4.02 ppm (H3, td). The chemical shifts for the remaining protons were δH 2.56 ppm (H4a, dd) and δH 2.90 ppm (H4b, dd), corresponding to the secondary protons of methylene (-CH2-). The 13C-NMR showed 15 signals, indicating the number of carbons in the structure of the isolated pure catechin compound. The DEPT 135 spectrum revealed that the isolated compound included seven tertiary carbons (δC 69.2, 82.6, 95.5, 96.3, 115.1, 115.2, and 120.0 ppm), seven quaternary carbons (δC 100.8, 132.1, 146.2, 147.2, 156.9, 157.5, and 157.8 ppm), and one secondary carbon (δC 28.4). The data obtained from the NMR spectra were further compared to the data from previous literature (Table 1). (The minor changes observed were due to the differences in the solvent used for the NMR analysis). From these findings, Compound 1 (Fig. 3) was identified as (+) Catechin with the molecular formula $C_{15}H_{14}O_6$.

3.2 Formation of inclusion complexes

3.2.1 Inclusion complex study

For the inclusion complex study of catechin with βCD and HPβCD, the absorption of catechin was observed before and after the addition of βCD and HPβCD. Before the addition, both βCD and HPβCD showed no absorption within 250 to 300 nm. After the addition of βCD and HPβCD to catechin, the absorption of catechin and the respective complexes remained unchanged. However, the intensities were observed to have increased (Fig. 4). This increase in intensity indicated the formation of inclusion complexes, with the HPβCD complex showing higher intensity compared to the βCD complex.[35]

3.2.2 Stoichiometry and Apparent Formation Constant of the Inclusion Complex

To determine the apparent formation constant of the inclusion complex of catechin with βCD and HPβCD, the concentration of catechin was maintained at 0.1 mM while the concentrations of βCD and HPβCD were increased. The absorbance of the solutions was measured at 236 nm against a reagent blank prepared with identical reagent concentrations but without catechin. The absorption spectra of the inclusion complex at different concentrations of βCD and HPβCD are shown in Fig. 5. It was observed that the absorbance value increased with increasing cyclodextrin concentration while the concentration of catechin remained constant. This indicates that the solubility of catechin increases upon forming the inclusion complex.

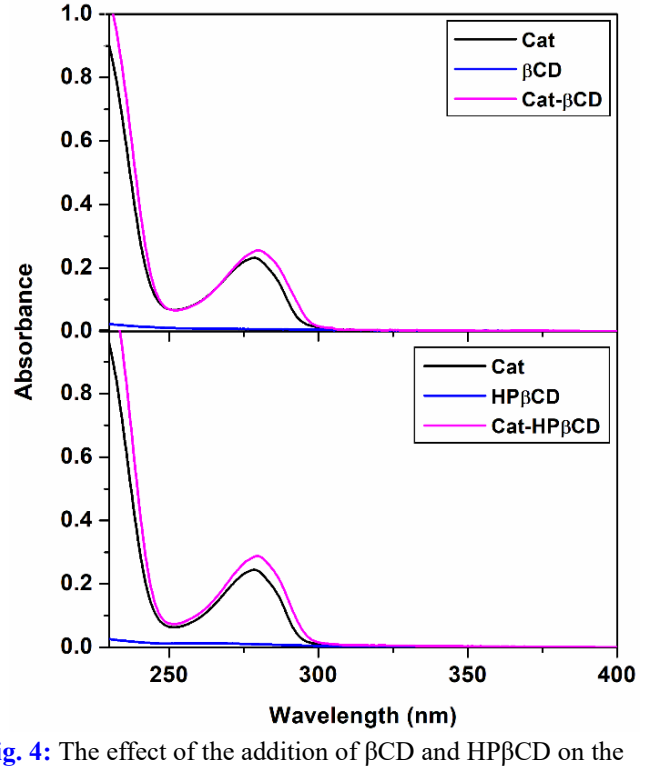

Fig. 4: The effect of the addition of βCD and HPβCD on the absorbance of Cat.

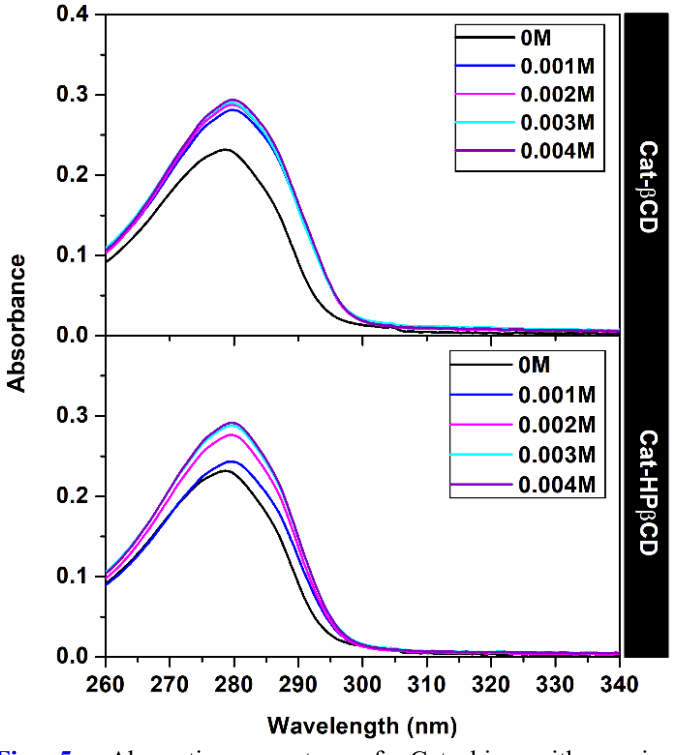

Fig 5: Absorption spectra of Catechin with various concentrations at pH 7, T = 25 °C. From lines 1 to 5: 0 M; 0.001 M; 0.002 M; 0.003 M and 0.004 M.

Based on the Benesi–Hildebrand equation, reciprocal plots for all the complexes were created to determine the relationship between 1/A and 1/[βCD] or 1/[HPβCD]. Good linear relationships were obtained for all complexes (Fig. 6), indicating that the stoichiometric ratios for all host-guest complexes were 1:1. Moreover, the formation constants (K) values suggested that catechin formed more stable and reliable inclusion complexes with HPβCD compared to native βCD, with K value of 16,973.5 g/mol and 16,868 g/mol, respectively.[36 37]

3.2.3 Field Emission Scanning Electron Microscopy (FESEM) Analysis

Field Emission Scanning Electron Microscopy (FESEM) was employed to examine the surface morphology of Cat, βCD, HPβCD, and their respective inclusion complexes. Pure Cat (Figs. 7a and 7b) exhibited a highly agglomerated needle-shaped crystal, characterized by irregular and compact clusters. This observation aligns with previous studies, which have reported catechin crystallizing in irregular plate-like, needle-like, or rod-like forms, contributing to its poor solubility and stability.[38,39] In contrast, βCD (Fig. 7c) displayed well-defined, block-like particles with a porous texture, consistent with the semi-crystalline nature of native cyclodextrins.[39,40] Similarly, HPβCD (Fig. 7d) exhibited a spherical, highly porous structure with a more fragmented appearance compared to βCD.[37 41] This morphological distinction is associated with enhanced solubility and dispersibility, corroborating previous findings that HPβCD possesses superior inclusion capacity due to its amorphous and disordered nature.[41,42]

The formation of catechin inclusion complexes resulted in significant morphological transformations compared to the individual components. For the Cat-βCD complex (Fig. 7e), the structure appeared more compact and homogenized, indicating successful interaction between catechin and βCD. The newly formed particles displayed reduced agglomeration and a smoother surface texture, which are indicative of partial inclusion and altered crystal habit.[43] The disappearance of catechin's crystalline features suggests that complex formation induced partial amorphization, a phenomenon previously observed in Cat-βCD inclusion complexes.[44] In the case of the Cat-HPβCD complex (Fig. 7f), a more pronounced transformation was observed. The original crystalline structure of catechin was no longer visible, replaced by a uniform, granular morphology. This morphology points to a well-encapsulated system with enhanced homogeneity, which may facilitate better aqueous dispersion and stability.[45] This indicates more efficient molecular dispersion within the HPβCD matrix. The observed morphological changes confirm the successful formation of Cat-βCD and Cat-HPβCD inclusion complexes.

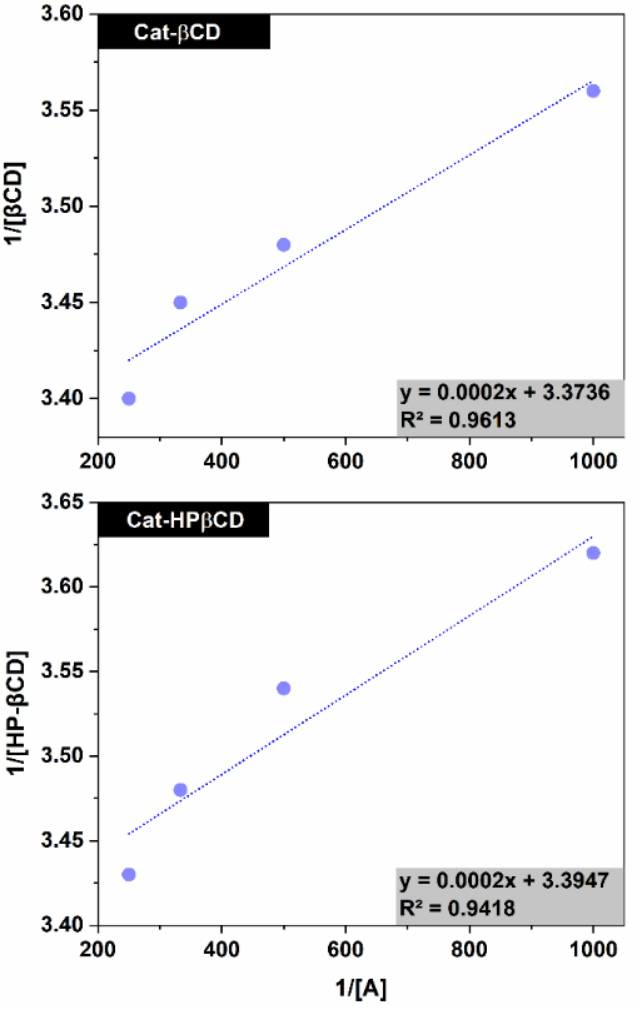

Fig 6: Reciprocal plot for 1/A against 1/[βCD and HPβCD] of inclusion complex.

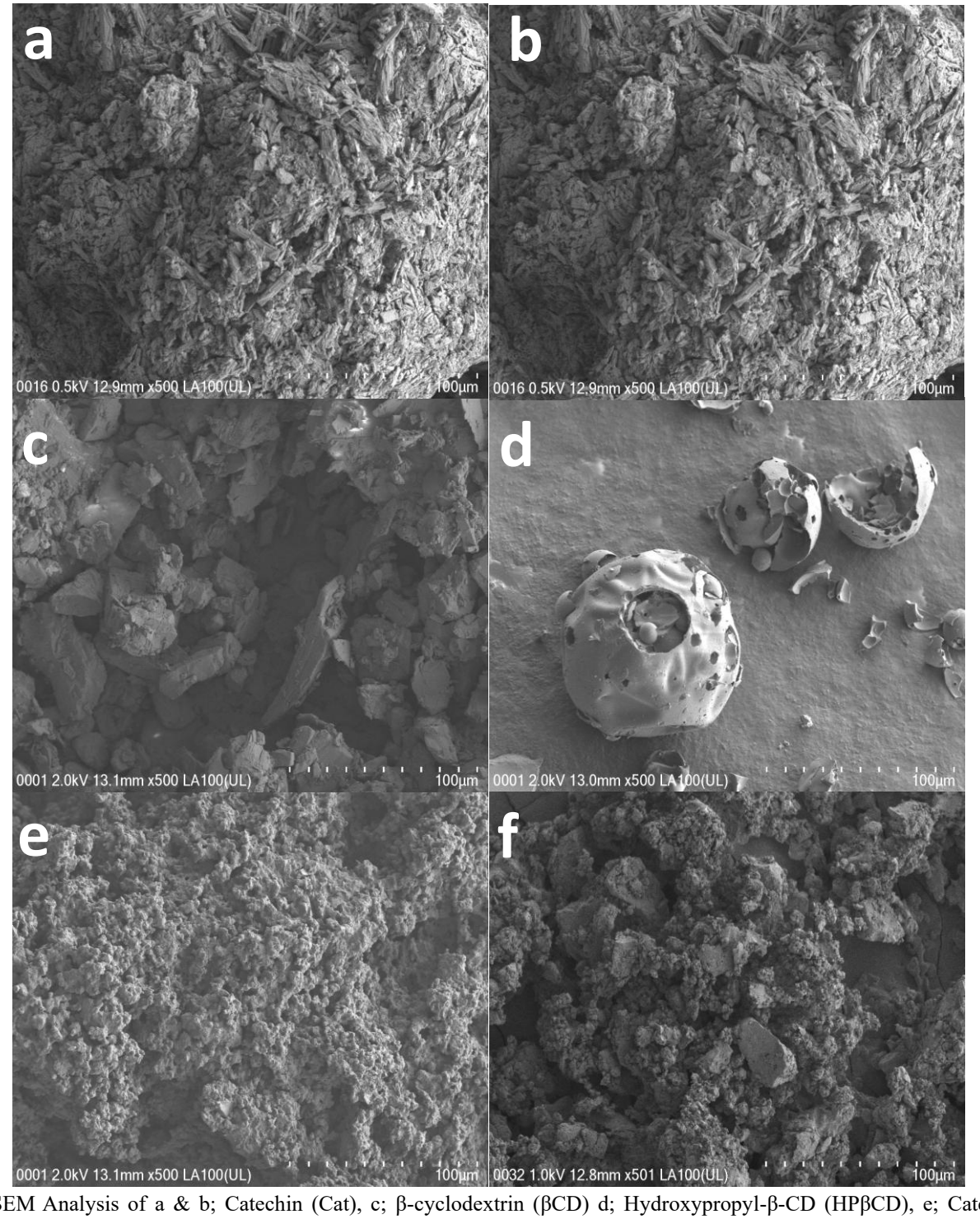

Fig. 7: FESEM Analysis of a & b; Catechin (Cat), c; β-cyclodextrin (βCD) d; Hydroxypropyl-β-CD (HPβCD), e; Catechin-β-cyclodextrin (Cat-βCD) and f; Catechin-hydroxypropyl-β-CD (Cat-HPβCD) complexes.

3.2.4 XRD characterization of catechin and cyclodextrin complexes

The X-ray diffraction (XRD) pattern of pure Cat (Figs. 8 & 9) exhibits sharp and intense diffraction peaks notably at peaks 2θ = 6.8◦, 9.2◦, 14.8◦, 15.2◦, 19.5◦, 21.5◦, 23.2◦, 24.9◦, 25.9◦,26.1◦, 27.5◦and 28.9◦, confirming its highly crystalline nature. This observation aligns with previous studies,[38,46] which have reported that catechin exists in a well-ordered molecular arrangement stabilized by strong intermolecular hydrogen bonding. These structural characteristics contribute to its poor solubility. In contrast, as shown in Fig. 8, the XRD profile of βCD reveals a semi-crystalline structure, characterized by broad diffraction peaks at approximately 2θ 9.2°, 12° and 18°. This pattern is consistent with earlier studies and reflects the semi-crystalline nature of βCD.[40,47,48] The XRD pattern of HPβCD (Fig. 9) demonstrates a more amorphous profile compared to βCD, with a significant reduction in peak intensity. This transformation from a semi-

crystalline to an amorphous state is attributed to hydroxypropyl substitution, which disrupts the ordered lattice structure of cyclodextrins.[37,38,41,42] This structural change (absence of sharp peaks) in HPβCD suggests enhanced molecular flexibility, improved complexation efficiency, and facilitated better dissolution and bioavailability as reported in previous studies.[42]

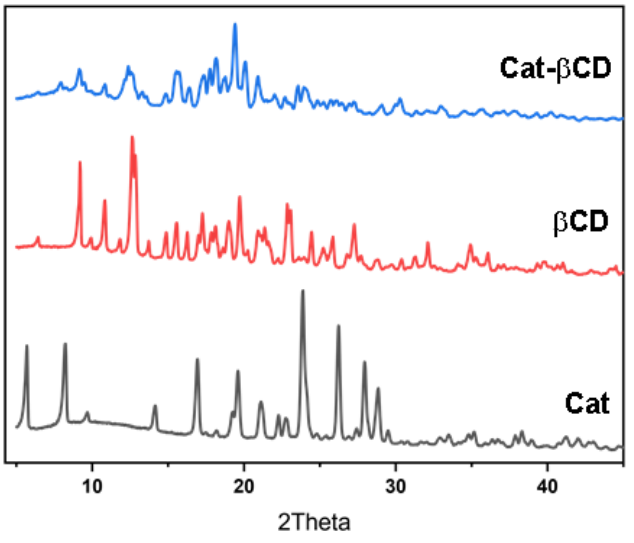

Fig. 8: XRD patterns of Cat (black line), βCD (red line), and Cat-βCD complex (blue line). Position of peaks reported in Angstrom (Å).

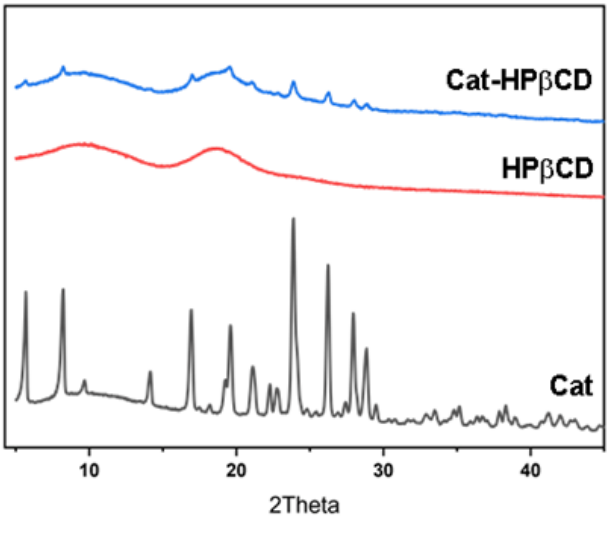

Fig. 9: XRD patterns of Cat (black line), HPβCD (red line), and Cat-HPβCD complex (blue line). Position of peaks reported in Angstrom (Å).

Overall, the XRD analysis highlights distinct differences in crystallinity among catechin, βCD, and HPβCD (Figs. 8 and 9), which significantly influence their complexation behavior. While catechin remains highly crystalline, its interaction with βCD results in partial peak reduction, indicating moderate inclusion complex formation. The presence of less intense and broader peaks in the Cat-βCD complex spectrum reflects a partial loss of crystallinity, suggesting that the host-guest interaction has disrupted the original crystal lattice of catechin.[48] In contrast, HPβCD exhibits a nearly amorphous structure, demonstrating superior encapsulation efficiency and solubility enhancement. Notably, the XRD pattern of the Cat-HPβCD complex lacks distinctive peaks, implying complete amorphization and successful molecular dispersion within the cyclodextrin matrix.[49] This trend is consistent with previous research, which has shown that amorphous cyclodextrins provide better molecular dispersion, leading to improved dissolution properties.[42] These findings underscore that HPβCD is a more effective carrier for catechin compared to βCD, owing to its enhanced molecular interactions and reduced crystallinity. The amorphous nature of HPβCD not only promotes stronger host–guest interactions but also contributes to improved pharmaceutical performance in terms of solubility and bioavailability.

3.2.5 ^{1}H-NMR analysis

^{1}H NMR spectroscopy is an effective technique for confirming the formation of inclusion complexes and can provide valuable insights into the inclusion mechanism of cyclodextrins (CDs) with guest molecules.[50,51] In this study, both the ^{1}H-NMR of the Cat and the CDs were dissolved in D_2O (Fig. 10).

As shown in Fig. 11, Chemical shift changes in chemical shift of specific nuclei in the host molecule can indicate the formation of an inclusion complex in solution (Table 2), as significant alterations are known to occur in the CD of the complex.[52] In the case of βCD, a pronounced upfield shift of the protons on H3, H5, and H6 (Ring B) was observed, suggesting that Ring B is situated within the inner cavity of the complex. In contrast, the H6 and H8 protons (Ring A) of βCD also experienced an upfield shift, but the changes were not as significant, indicating that Ring A is positioned on the outer part of the cavity (Fig. 8). For HPβCD, a substantial upfield shift was observed for the protons on H6, and H8 (Ring A), suggesting that Ring A is located in the inner cavity of the complex. Conversely, the H3, H5, and H6 protons (Ring B) of HPβCD also showed an upfield shift, but without considerable changes, indicating that Ring B is positioned on the outer part of the cavity (Fig. 12).

3.3 Molecular studies of inclusion complex

3.3.1. Initial conformation

Molecular docking was executed to obtain the initial conformation of Cat as guest toward βCD and HPβCD as host material. The docking results show that Cat has two favorable conformations within the cavity of both materials. Noted, the host material structure is a truncated cone shape, with the narrow rim (O6) indicated by the primary side and the wider rim (O2) indicated by the secondary side (Fig. 1b). The Ring-B of Cat is oriented toward to the narrow rim of βCD. Conversely, in the HPβCD complex, the B-ring is positioned near the wider rim (Fig. 12), which allows for deeper insertion and more favourable hydrogen bonding interactions. This

Table 2: The chemical shifts (δ) of Cat, βCD, and HPβCD, Cat complexes and their complexation shifts (Δδ).

Compound	Chemical Shift/Δδ (ppm)				
	H2’	H5’	H6’	H6	H8
Cat	6.90	6.88	6.81	6.06	5.95
Cat-βCD	6.79	6.74	6.69	6.05	5.93
Δδ*	0.11	0.14	0.12	0.01	0.02
Cat-HPβCD	6.87	6.86	6.76	5.99	5.80
Δδ*	0.03	0.02	0.05	0.17	0.15

Note: $\Delta\delta^* = \delta_{Cat} - \delta_{complex}$.

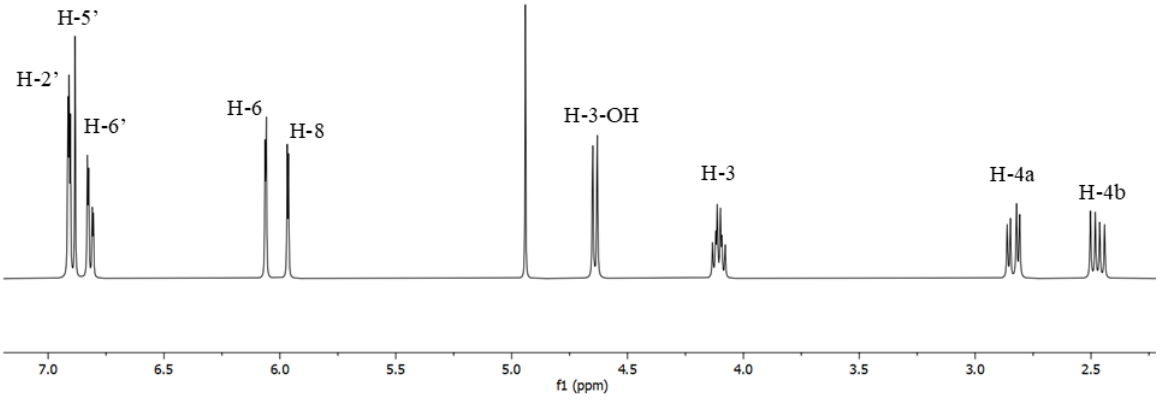

Fig. 10: ^{1}H-NMR spectra of (+) catechin in D_2O.

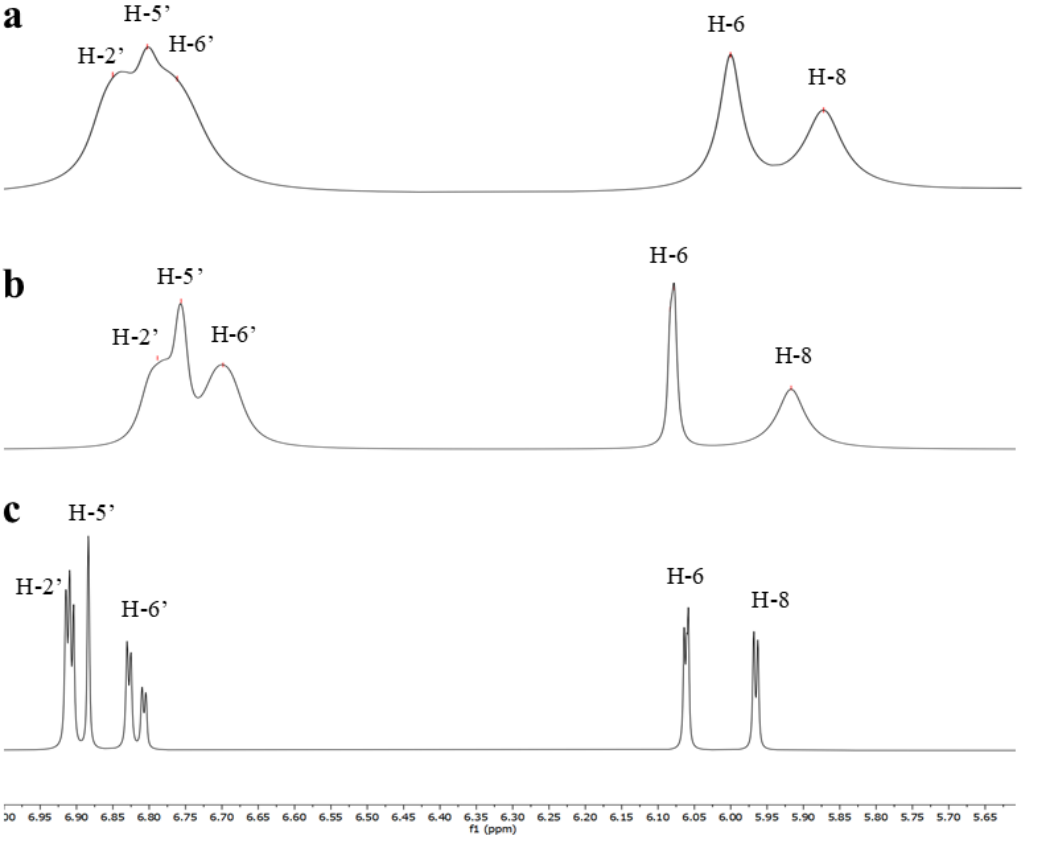

Fig. 11: ^{1}H-NMR spectra: (a) Cat-HPβCD; (b) Cat-βCD; and (c) Cat.

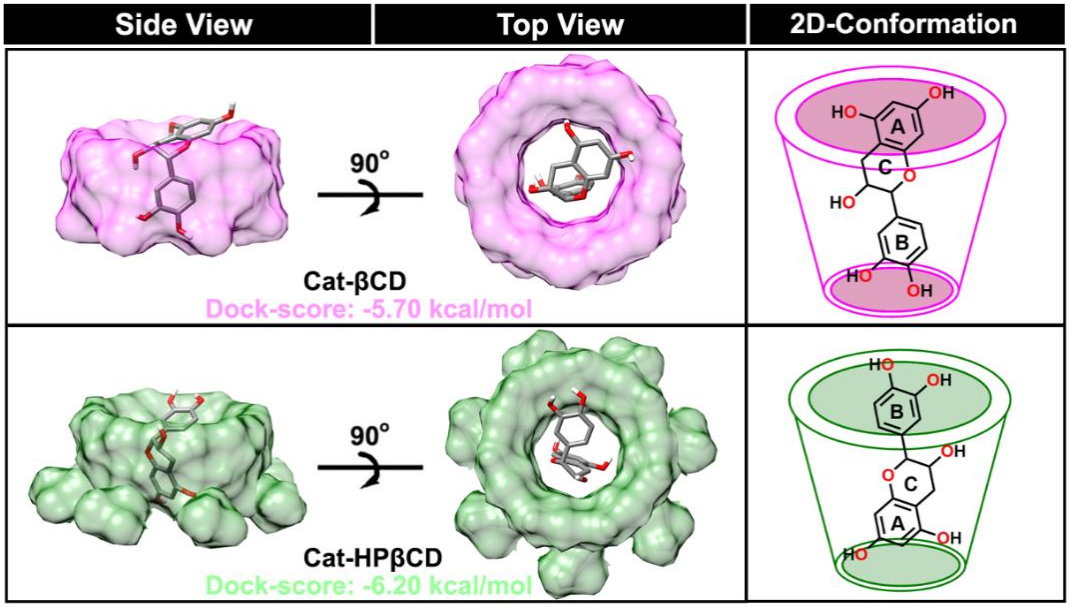

Fig. 12: Molecular docking result: Visualization of selected conformations with their energy interaction. The inclusion complexes with different conformations are shown in 2-dimension.

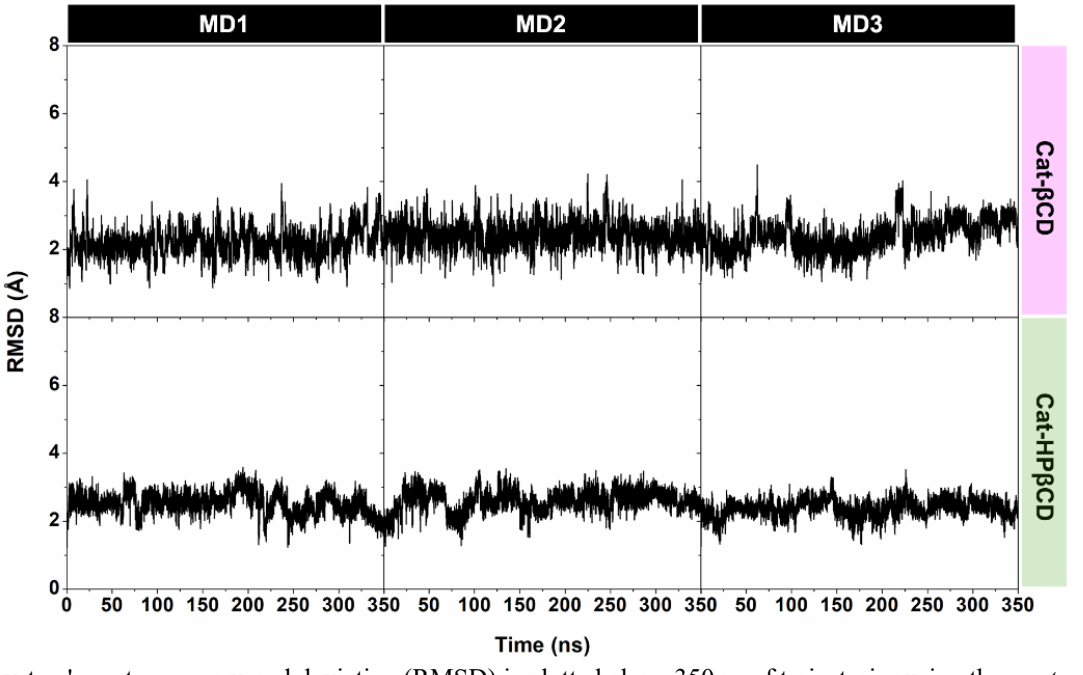

Fig. 13: Each system's root-mean-squared deviation (RMSD) is plotted along 350 ns of trajectories using the *cpptraj* tool.

statement is supported by their dock scores with Cat-βCD: -5.70 kcal/mol) and Cat-HPβCD (-6.20 kcal/mol). Next, we chose the best conformation for these conformations according to the lowest dock score as the initial structure from molecular docking for MD simulation purposes. Naturally, the lowest dock score provides better confirmation.[53] Overall, both conformations are well occupied within the cavity of cyclodextrins (CDs). For evaluation, the obtained conformation from this step is continued for further analysis via MD simulation.

3.3.2 System stability

To evaluate the stability of the inclusion complexes, several parameters were analyzed, including total energy (E_{total}), temperature, root-mean-square deviation (RMSD), radius of gyration (RoG), center-of-mass distance, and hydrogen bonding (H-bond) interactions.[54] The RMSD profiles revealed that both Cat-βCD and Cat-HPβCD systems maintained low fluctuations below 4 Å throughout the 350 ns simulations (Fig. 13), indicating well-stabilized complexes. These results are consistent with previous studies showing that cyclodextrin-based host systems exhibit stable RMSD profiles when complexed with small molecules.[55]

As mentioned in molecular docking (Fig. 12), the Cat conformation in the cavity of both CDs has an opposite orientation. This orientation difference is reflected in the

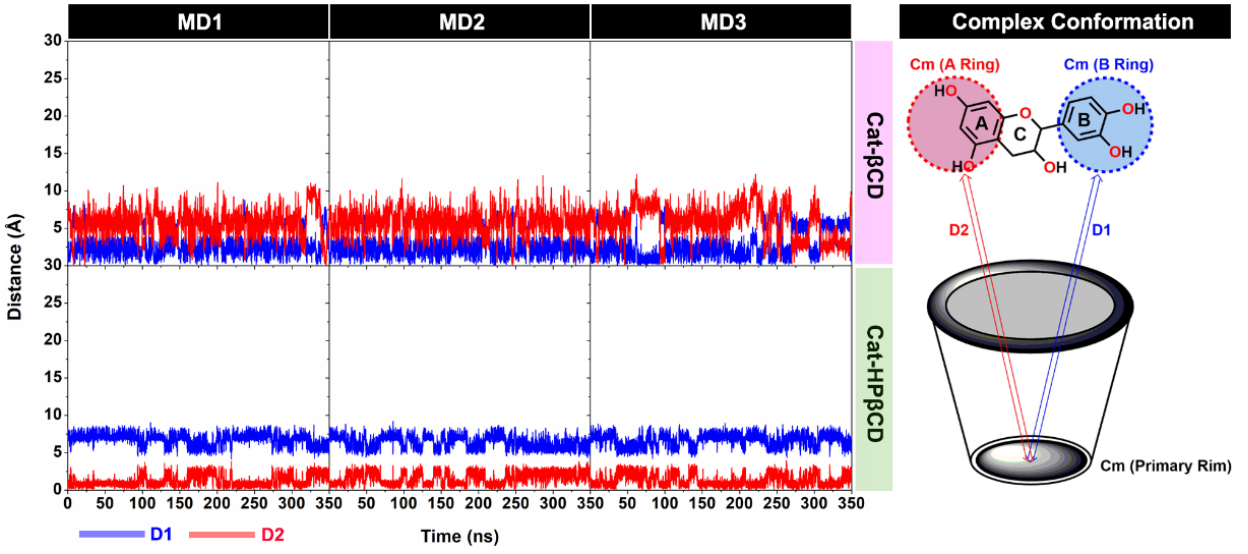

Fig. 14: The distance variable is plotted along 350 ns of trajectories using the *cpptraj* tool, where d[C_m (primary rim)-C_m(Ring-B)] (D1) and d[C_m (primary rim)-C_m(Ring-A)] (D2) are colored in blue and red, respectively.

distance measurements between catechin and the cyclodextrin cavity rims. Specifically, for Cat-βCD, D1 and D2 averaged 2.64 ± 1.46 Å and 5.81 ± 1.82 Å, respectively, while for Cat-HPβCD, the values were reversed, at 6.62 ± 0.81 Å and 1.40 ± 0.78 Å (Fig. 14).

To further assess positional stability, the distance between Cat (Ring-A or Ring-B) and primary ring was measured. It aimed to ensure the coordinates of the Cat stayed in the cavity. Moreover, the compactness of the inclusion complex was measured through the RoG variable (Fig. 15). The RoG variations ranged from ~5.56 to ~6.39 Å, indicating a well-inclused between guest and host of each complex. The trend in RoG matched with RMSD, indicating good stability of these variables. Our findings suggest the inclusion complex of Cat-βCD and Cat-HPβCD achieved good stability and binding coordinates that did not change significantly over the MD simulation.

Molecular interactions are analyzed along the trajectories generated during the simulation time that showed by the hydrogen bond (Hbond) variable (Fig. 16). The H-bond formation was considered by using a distance < 3.5 Å and an angle < 120º. The results show that Cat-HPβCD has more interaction than Cat-βCD over the simulation. This observation aligns with the more favourable positioning of catechin within the HPβCD cavity, which, due to its hydroxypropyl substitutions, offers enhanced flexibility and a more hydrophilic environment conducive to hydrogen bonding. The deeper insertion of catechin into HPβCD enables better spatial alignment of its hydrogen bond donor and acceptor groups, including phenolic –OH and ether functionalities, thereby increasing the frequency and persistence of H-bond formation.

It should be noted, that, Hydrogen bonding plays a critical role in stabilizing inclusion complexes, enhancing both the retention and orientation of guest molecules within cyclodextrin cavities.[56] The greater number of H-bonds observed in the Cat-HPβCD complex supports the view that its conformational orientation contributes to its superior stability over time. These results collectively confirm that both complexes are stable, with the HPβCD complex demonstrating enhanced host–guest interactions attributable to its conformational and structural features.

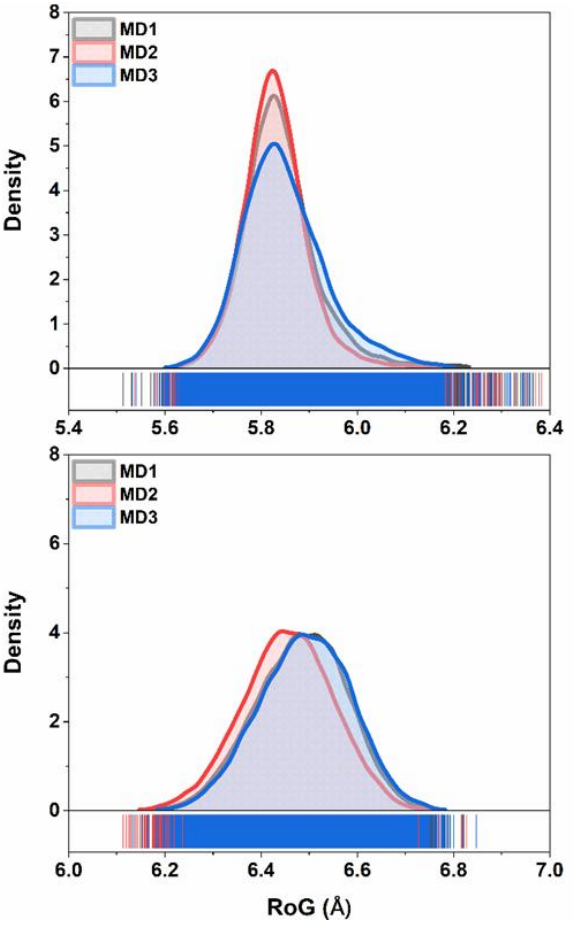

Fig. 15: The radius of gyration (RoG) variable is plotted along 350 ns of trajectories using the *cpptraj* tool. The RoG distribution is plotted using kernel smoothing.

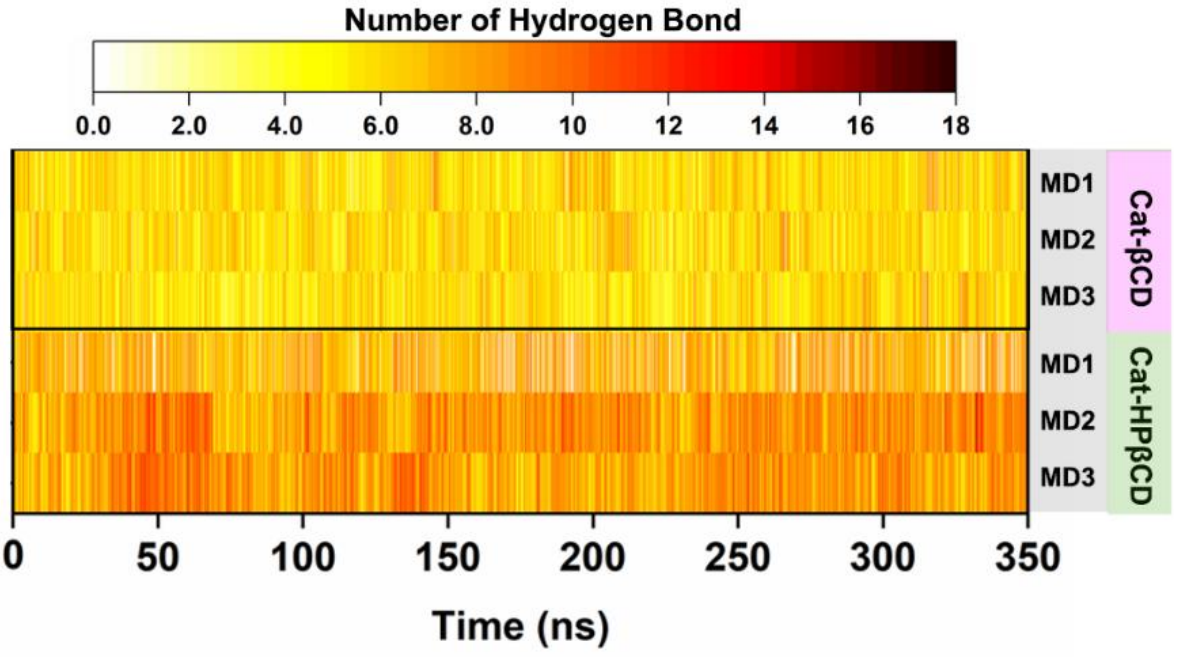

Fig. 16: Molecular interaction between Cat and CDs is plotted over 350 ns of trajectories. Cut value of H-bond (distance < 3.5 Å and angle < 120°). The number of interactions is colored from the lowest (white) to the highest (brown).

Table 3: Energy components (kcal/mol) of inclusion complexes estimated with MM-GBSA, MM-PBSA, and QM/MM-GBSA approaches. Data are shown as mean ± standard error of the mean (SEM).

Energy Component	Cat-βCD			Cat-HPβCD		
	MD1	MD2	MD3	MD1	MD2	MD3
Gas Term						
$\Delta G_{gas(MM)}$	-36.02 ± 0.18	-34.91 ± 0.16	-40.58 ± 0.18	-43.18 ± 0.16	-44.57 ± 0.14	-41.75 ± 0.16
$\Delta G_{gas(QM)}$	-27.20 ± 0.18	-27.98 ± 0.08	-26.84 ± 0.08	-35.17 ± 0.08	-36.03 ± 0.07	-34.61 ± 0.07
Solvation (GBSA)						
$\Delta G_{sol\ (MM\text{-}GBSA)}$	16.01 ± 0.14	15.19 ± 0.10	17.68 ± 0.10	18.93 ± 0.11	19.78 ± 0.10	18.15 ± 0.11
$\Delta G_{sol\ (MM\text{-}PBSA)}$	18.58 ± 0.12	17.85 ± 0.10	20.26 ± 0.10	18.57 ± 0.12	19.21 ± 0.10	17.79 ± 0.11
$\Delta G_{sol\ (QM\text{-}GBSA)}$	20.66 ± 0.13	20.30 ± 0.12	21.79 ± 0.12	25.24 ± 0.12	26.45 ± 0.12	24.50 ± 0.13
Enthalpy						
$\Delta H_{(MM\text{-}GBSA)}$	-20.01 ± 0.09	-19.72 ± 0.08	-22.90 ± 0.10	-24.24 ± 0.08	-24.78 ± 0.07	-23.59 ± 0.08
$\Delta H_{(MM\text{-}PBSA)}$	-17.44 ± 0.10	-17.05 ± 0.09	-20.32 ± 0.11	-24.60 ± 0.10	-25.35 ± 0.08	-23.95 ± 0.09
$\Delta H_{(QM/MM\text{-}GBSA)}$	-17.54 ± 0.09	-17.50 ± 0.08	-19.92 ± 0.10	-20.50 ± 0.08	-21.05 ± 0.08	-19.96 ± 0.07
Entropy						
$-T\Delta S$	-16.43 ± 0.12	-15.94 ± 0.10	-18.14 ± 0.12	-18.22 ± 0.12	-18.55 ± 0.13	-18.00 ± 0.14
Binding Free Energy						
$\Delta G_{bind(MM\text{-}GBSA)}$	-3.58	-3.77	-4.76	-6.02	-6.23	-5.59
$\Delta G_{bind(MM\text{-}PBSA)}$	-1.01	-1.10	-2.18	-6.38	-6.80	-5.95
$\Delta G_{bind(QM/MM\text{-}GBSA)}$	-1.11	-1.55	-1.78	-2.28	-2.50	-1.96

3.3.3 Free energy binding

To estimate the binding affinity of the inclusion complexes, binding free energy (ΔG_{bind}) was calculated using three approaches: MM-GBSA, MM-PBSA, and QM/MM-GBSA. A total of 5000 snapshots were extracted from the last 100 ns of the MD trajectories for each system. The energy components obtained from these methods are summarized in Table 3. Thermodynamically, a more negative (ΔG_{bind}) value indicates a stronger interaction between the guest (Cat) and host (βCD or HPβCD). This binding affinity is influenced by contributions from the gas-phase interaction energy (ΔG_{gas}) and solvation energy (ΔG_{sol}), which collectively determine the thermodynamic stability of the inclusion complexes.[57,58]

Among the components, the gas-phase interaction energy ΔG_{gas} made the most significant contribution to ΔG_{bind}. While the solvation energies ΔG_{sol} derived from both GB and PB showed only minor variations between complexes, notable differences were observed in the enthalpy (ΔH) values, which significantly influenced the final binding energy values. Entropic contributions ($-T\Delta S$), on the other hand, were

comparable across all systems. The overall ΔG_{bind} values from all approaches consistently indicated that the Cat-HPβCD complex exhibits a stronger binding affinity than the Cat-βCD complex. These results are congruent with previously observed trends in docking scores (Fig. 12) and formation constants (Fig. 6). Collectively, these findings suggest that HPβCD forms a more stable and thermodynamically favourable inclusion complex with Cat compared to βCD. This is supported by stronger binding affinity, increased hydrogen bonding interactions, and higher structural stability during the simulation period. The superior binding performance of HPβCD highlights its potential as a promising carrier to enhance the solubility and bioavailability of Cat in drug delivery applications.

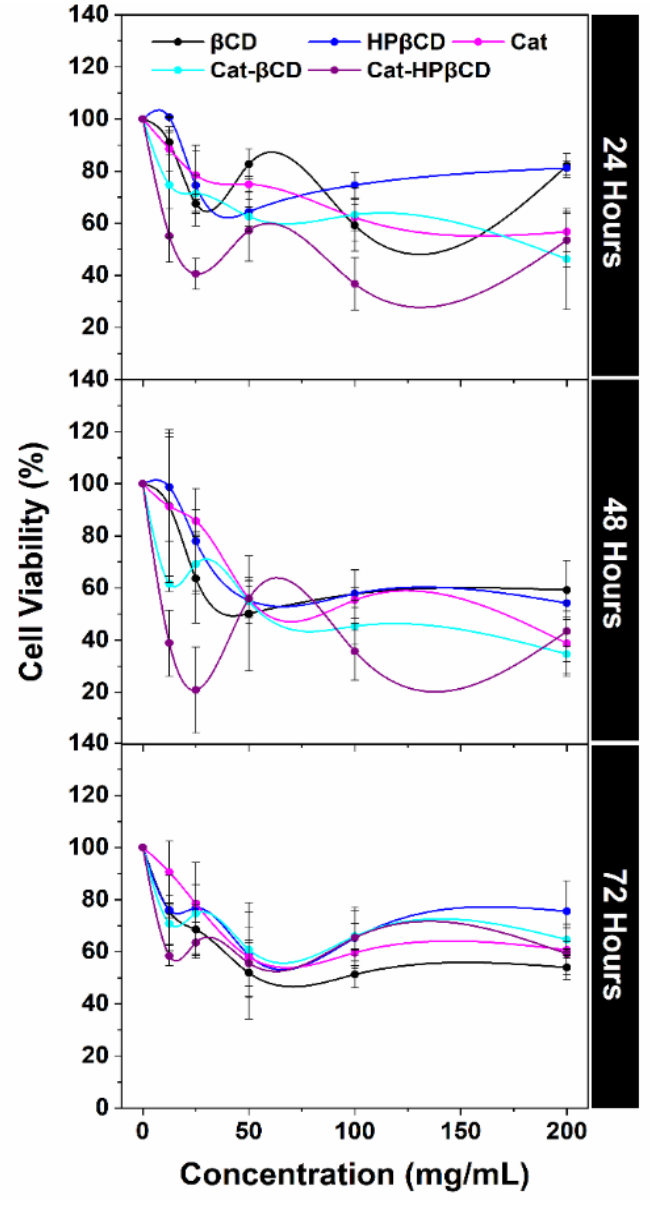

Fig. 17: Cell viability of MCF-7 cells using MTT assay. The dose-response curves of treatment for 24, 48, and 72h, respectively. The cells were treated with various concentrations of βCD, HPβCD, Cat, Cat-βCD, and Cat-HPβCD.

3.4 Inclusion complex enhances the inhibition of breast cancer cell

In this study, we observed that Cat-HPβCD was the only compound among the tested formulations that significantly reduced cell viability in MCF-7 cells. While the initial 24-hour treatment did not result in a notable decrease in cell viability or achieve an IC_{50} value, prolonged exposure to Cat-HPβCD for 48 and 72 hours showed a marked reduction in cell viability. Specifically, the IC_{50} values were determined to be 14 µg/mL at 48 hours and 10 µg/mL at 72 hours (Fig. 17). This indicated a time-dependent increase in the cytotoxic effect of Cat-HPβCD on MCF-7 cells. However, at concentrations exceeding the IC_{50} values, an unexpected recovery in cell viability was observed, suggesting that MCF-7 cells may invoke compensatory mechanisms to resist high-dose toxicity. Previous literature has reported similar biphasic dose-responses, which was linked to stress-induced survival pathways such as PI3K/Akt or Nrf2-mediated signalling.[59] Although no additional gene expression or protein-based assays were performed in this study, future investigations involving RT-qPCR or Western blot analysis targeting pro-survival genes and oxidative stress markers could help clarify the molecular mechanisms behind this adaptive response.[60]

The findings from this cell viability assay suggest that Cat-HPβCD possesses cytotoxic properties against MCF-7 breast cancer cells, particularly with increased exposure time. The fact that Cat-HPβCD was the only compound to reduce cell viability effectively highlights its potential as a lead compound for further investigation in cancer therapeutics. The absence of an IC_{50} value at 24 hours, followed by the attainment of IC_{50} values at 48 and 72 hours, indicates that the compound's cytotoxic effects are not immediate but build over time. This delayed response could be attributed to the time required for the compound to exert its effects on critical cellular processes.

The observed recovery of cells at higher concentrations suggests that MCF-7 cells may activate survival pathways in response to high doses of Cat-HPβCD. This speculation is supported by reports of hormetic responses in cancer cells, where low and high concentrations of a compound yield different cellular outcomes due to adaptive stress responses.[61] Although, this phenomenon warrants further investigation to elucidate the underlying mechanisms, which could involve alterations in gene expression or activation of drug efflux pumps.[62] The lack of cytotoxicity observed with the other compounds, including βCD, HPβCD, and Cat, implies that the combination of HPβCD with Cat may be crucial for its enhanced efficacy. The potential synergistic effects between HPβCD and Cat should be further explored to optimize the formulation and improve its therapeutic index.

4. Conclusion

This study successfully isolated catechin from the sap of *Uncaria gambir* and enhanced its solubility through molecular encapsulation with β-cyclodextrin (βCD) and hydroxypropyl-β-cyclodextrin (HPβCD). The formation constant of the

complexes revealed that Cat-HPβCD (16,973.5 g/mol) exhibited a higher stability than Cat-βCD (16,868 g/mol), suggesting superior encapsulation efficiency. Computational studies, including molecular docking and molecular dynamics simulations, further confirmed that catechin forms stronger and more stable interactions with HPβCD, as indicated by higher docking scores and binding free energy (ΔG_{bind}). The biological evaluation demonstrated that Cat-HPβCD exhibited significant time-dependent cytotoxic effects against MCF-7 breast cancer cells, with IC_{50} values at 48 and 72 hours, indicating enhanced anticancer activity. However, the observed recovery of cell viability at higher concentrations suggests a complex biological response that may involve resistance mechanisms or adaptive survival pathways. These preliminary findings underscore the promise of HPβCD as a delivery system for catechin, yet further studies—particularly in vivo evaluations and molecular pathway analyses are necessary to fully understand its therapeutic potential and limitations. Overall, the findings of this study strongly support HPβCD as a superior encapsulation material for catechin, significantly enhancing its solubility, stability, and anticancer activity, making it a promising candidate for future pharmaceutical development.

Acknowledgements
This study was supported by the Research Program of "INTERNATIONAL RESEARCH COLLABORATION TOP #100 UNIVERSITAS AIRLANGGA, 2024" from Universitas Airlangga. Contract Number: 382/UN3.LPPM/PT.01.03/2024. Additionally, we are grateful for the computational resources for this work supported by the Biotechnology of Tropical Medicinal Plants Research Group, Universitas Airlangga.

Conflict of interest
There are no conflicts to declare.

Supporting information
Applicable.

Reference
[1] D. Nandika, K. Syamsu, Arinana, D. T. Kusumawardhani, Y. Fitriana, Bioactivities of catechin from Gambir (Uncaria gambir Roxb.) against wood-decaying fungi, *BioResources*, 2019, **14**, 5646-5656, doi: 10.15376/biores.14.3.5646-5656.
[2] A. P. Davis, E. Figueiredo, A checklist of the Rubiaceae (coffee family) of Bioko and Annobon (Equatorial Guinea, Gulf of Guinea), *Systematics and Biodiversity*, 2007, **5**, 159-186, doi: 10.1017/S1477200006002143.
[3] T. Anggraini, A. Tai, T. Yoshino, T. Itani, Antioxidative activity and catechin content of four kinds of Uncaria gambir extract from West Sumatra, *African Journal of Biochemistry Research*, 2011, **5**, 33-38, doi: 10.5897/AJBR.9000033.
[4] M. Amir, M. Mujeeb, A. Khan, K. Ashraf, D. Sharma, M. Aqil, Phytochemical analysis and in vitro antioxidant activity of Uncariagambir, *International Journal of Green Pharmacy*, 2012, **6**, 67-72, doi: 10.4103/0973-8258.97136.
[5] S. Reuter, S. C. Gupta, M. M. Chaturvedi, B. B. Aggarwal, B. B. Oxidative stress, inflammation, and cancer: How are they linked?, *Free Radical Biology and Medicine*, 2010, **49**, 1603–1616. doi: 10.1016/j.freeradbiomed.2010.09.006
[6] A. Federico, F. Morgillo, C. Tuccillo, F. Ciardiello, C. Loguercio. Chronic inflammation and oxidative stress in human carcinogenesis, *International Journal of Cancer*, 2007, **121**, 2381–2386. doi: 10.1002/ijc.23192
[7] R. Ahmad, H. H.M, N. Z.M, I. N.H, S. F, L. N.H, S. K., The Antioxidant & Antidiabetic of Potential Uncaria, *Research Journal of Medicinal Plant*, 2011, **5**, 287-595, doi: 10.3923/RJMP.2011.587.595.
[8] A. S. Ismail, Y. Rizal, Armenia, A. Kasim, Hyptis verticillata Jacq: A review of its traditional uses extension, phytochemistry, pharmacology, and toxicology, *Biodiversitas*, 2021, **22**, 1474-1480, doi: 10.13057/BIODIV/D220351.
[9] D. Stelzle, L. F. Tanaka, K. K. Lee, A. Ibrahim Khalil, I. Baussano, A. S. V. Shah, D. A. McAllister, S. L. Gottlieb, S. J. Klug, A. S. Winkler, F. Bray, R. Baggaley, G. M. Clifford, N. Broutet, S. Dalal. Estimates of the global burden of cervical cancer associated with HIV, *Lancet Global Health*, 2021, **9**, e161-e169, doi: 10.1016/S2214-109X(20)30459-9.
[10] A. Musa, M. I. Abdjan, N. S. Aminah, A. Novi, A. Laurens, L. Windah, A. Saiful, I. Anticancer potential of 3-O-methylellagic acid 3'-O-α-rhamnoside from shorea beccariana: In silico studies, *Journal of Medicinal and Chemical Sciences*, 2024, **7**, 1062-1074, doi: 10.26655/JMCHEMSCI.2024.8.7.
[11] A. Musa, N. S. Aminah, A. N. Kristanti, I. fathoni, R. T. Amalia, T. M. Thant, P. Rajasulochana, Y. Takaya, Phytochemical and pharmacological profile of genus Shorea : A review of the recent literature, *Heliyon*, 2024, **10**, 1-23, doi: 10.1016/j.heliyon.2023.e23649.
[12] C. S. Yang, Z. Y. Wang. Tea and Cancer, *Journal of the National Cancer Institute*, 1993, **85**, 1038-1049, doi: doi:10.1093/jnci/85.13.1038.
[13] Z. Y. Chen, Q. Y. Zhu, D. Tsang, Y. Huang, Degradation of green tea catechins in tea drinks, *Journal of Agricultural and Food Chemistry*, 2001, **49**, 477-482, doi: 10.1021/jf000877h.
[14] M. E. Heitzman, C. C. Neto, E. Winiarz, A. J. Vaisberg, G. B. Hammond. Ethnobotany, phytochemistry, and pharmacology of Uncaria (Rubiaceae), *Phytochemistry*, 2005, **66**, 5-29, doi: 10.1016/j.phytochem.2004.10.022.
[15] J. Ze Xu, S. Y. Venus Yeung, Q. Chang, Y. Huang, Z. Y. Chen, Comparison of antioxidant activity and bioavailability of tea epicatechin with their epimers, *British Journal of Nutrition*, 2004, **91**, 873-881, doi: 10.1079/bjn20041132.
[16] K.R. Chagam, E. S. Jung, S. Y., Son, C. H. Lee. Inclusion complexation of catechins-rich green tea extract by β-cyclodextrin: Preparation, physicochemical, thermal, and antioxidant properties, *LWT-Food Science and Technology*, 2020, **131**, 109723. doi: 10.1016/j.lwt.2020.109723
[17] R. L. Abarca, F. J. Rodríguez, A. Guarda, M. J. Galotto, J. E. Bruna. Characterization of beta-cyclodextrin inclusion complexes containing an essential oil component, *Food*

Chemistry, 2016, **196**, 968-975. doi: 10.1016/j.foodchem.2015.10.023.
[18] A. P. Wardana, N. S. Aminah, A. N. Kristanti, M. Z. Fahmi, H. I. Zahrah, W. Widiyastuti, H. A. Ajiz, U. Zubaidah, P. A. Wiratama, Y. Takaya, Nano Uncaria gambir as Chemopreventive Agent Against Breast Cancer, *International Journal of Nanomedicine*, 2023, **18**, 4471-4484, doi: 10.2147/IJN.S403385.
[19] V. Crupi, R. Ficarra, M. Guardo, D. Majolino, R. Stancanelli, V. Venuti, UV–vis and FTIR–ATR spectroscopic techniques to study the inclusion complexes of genistein with β-cyclodextrins, *Journal of Pharmaceutical and Biomedical Analysis*, 2007, **44**, 110-117, doi: 10.1016/j.jpba.2007.01.054.
[20] S. Mohamad, H. Surikumaran, M. Raoov, T. Marimuthu, K. Chandrasekaram, P. Subramaniam, Conventional study on novel dicationic ionic liquid inclusion with β-cyclodextrin, *International Journal of Molecular Sciences*, 2011, **12**, 1-17, doi: 10.3390/ijms12096329.
[21] J. J. T. L. M.T. Esclusa-Diaz, M. Guimaraens-Mfndez, M.B. Pfrez-Marcos, J.L. Vila-Jato, Characterization and in vitro dissolution behaviour of ketoconazole/β and 2-hydroxypropyl-β-cyclodextrin inclusion compounds, *International Journal of Pharmaceutics*, 1996, **5173**, 203-210, doi: 10.1016/S0378-5173(96)04704-7.
[22] S. Mohamad, K. Chandrasekaram, F. L. M. Rasdi, N. S. A. Manan, M. Raoov, N. Sidek, S. F. Fathullah, Supramolecular interaction of 2,4-dichlorophenol and β-cyclodextrin functionalized ionic liquid and its preliminary study in sensor application, *Journal of Molecular Liquids*, 2015, **212**, 850-856, doi: 10.1016/j.molliq.2015.10.044.
[23] A. J. Cohen, P. Mori-Sąnchez, W. Yang, Challenges for density functional theory, *Chemical Reviews*, 2012, **112**, 289-320, doi: 10.1021/cr200107z.
[24] A. Oo, K. Kerdpol, P. Mahalapbutr, T. Rungrotmongkol, Molecular encapsulation of emodin with various β-cyclodextrin derivatives: A computational study, *Journal of Molecular Liquids*, 2022, **347**, 1-9, doi: 10.1016/j.molliq.2021.118002.
[25] S. Genheden, U. Ryde, The MM/PBSA and MM/GBSA methods to estimate ligand-binding affinities, *Expert Opinion on Drug Discovery*, 2015, **10**, 449-461, doi: 10.1517/17460441.2015.1032936.
[26] D. A. Case, T. E. Cheatham, T. Darden, H. Gohlke, R. Luo, K. M. Merz, A. Onufriev, C. Simmerling, B. Wang, R. J. Woods, The Amber biomolecular simulation programs, *Journal of Computational Chemistry*, 2005, **26**, 1668-1688, doi: 10.1002/jcc.20290.
[27] D. A. Case, H. M. Aktulga, K. Belfon, D. S. Cerutti, G. A. Cisneros, V. W. D. Cruzeiro, N. Forouzesh, T. J. Giese, A. W. Götz, H. Gohlke, S. Izadi, K. Kasavajhala, M. C. Kaymak, E. King, T. Kurtzman, T. S. Lee, P. Li, J. Liu, T. Luchko, R. Luo, M. Manathunga, M. R. Machado, H. M. Nguyen, K. A. O'Hearn, A. V. Onufriev, F. Pan, S. Pantano, R. Qi, A. Rahnamoun, A. Risheh, S. Schott-Verdugo, A. Shajan, J. Swails, J. Wang, H. Wei, X. Wu, Y. Wu, S. Zhang, S. Zhao, Q. Zhu, T. E. Cheatham, D. R. Roe, A. Roitberg, C. Simmerling, D. M. York, M. C. Nagan, K. M. Merz, AmberTools, *Journal of Chemical Information and Modeling*, 2023, **63**, 6183-6191, doi: 10.1021/acs.jcim.3c01153.
[28] J. Wang, R. M. Wolf, J. W. Caldwell, P. A. Kollman, D. A. Case, Development and testing of a general Amber force field, *Journal of Computational Chemistry*, 2004, **25**, 1157-1174, doi: 10.1002/jcc.20035.
[29] B. A. Luty, W. F. Van Gunsteren. Calculating electrostatic interactions using the particle-particle particle-mesh method with nonperiodic long-range interactions, *Journal of Physical Chemistry*, 1996, **100**, 2581-2587, doi: 10.1021/jp9518623.
[30] T. Lee, D. S. Cerutti, D. Mermelstein, C. Lin, S. Legrand, J. Giese, A. E. Roitberg, D. A. Case, R. C. Walker, D. M. York, Ross, in Amber18 : performance enhancements and new features GPU-accelerated molecular dynamics and free energy methods in Amber18 : performance enhancements and new features, *Journal of Chemical Information and Modeling*, 2018, **58**, 2043-2050, doi: 10.1021/acs.jcim.8b00462.
[31] D. R. Roe, T. E. Cheatham, PTRAJ and CPPTRAJ: Software for processing and analysis of molecular dynamics trajectory data, *Journal of Chemical Theory and Computation*, 2013, **9**, 3084-3095, doi: 10.1021/ct400341p.
[32] B. R. Miller, T. D. McGee, J. M. Swails, N. Homeyer, H. Gohlke, A. E. Roitberg, MMPBSA.py: An efficient program for end-state free energy calculations, *Journal of Chemical Theory and Computation*, 2012, **8**, 3314-3321, doi: 10.1021/ct300418h.
[33] M. Ghasemi, T. Turnbull, S. Sebastian, I. Kempson, Rapid colorimetric assay for cellular growth and survival: Application to proliferation and cytotoxicity assays, *International Journal of Molecular*, 2021, **22**, 1-30, doi: 10.3390/ijms222312827.
[34] P. P. Acharya, G. R. Genwali, M. Rajbhandari, Isolation of catechin from Acacia catechu willdenow estimation of total flavonoid content in Camellia sinensis Kuntze and Camellia sinensis Kuntze var. assamica collected from different geographical region and their antioxidant activities, *Scientific World*, 2013, **11**, 32-36, doi: 10.3126/sw.v11i11.8549.
[35] R. Patel, N. Purohit, Physicochemical characterization and in vitro dissolution behavior of nicardipine–cyclodextrins inclusion compounds, *AAPS PharmSciTech*, 2009, **10**, 1301-1312, doi: 10.1208/s12249-009-9321-3.
[36] Y. Gao, X. Zhao, B. Dong, L. Zheng, N. Li, S. Zhang, Inclusion complexes of beta-cyclodextrin with ionic liquid surfactants, *Journal of Physical Chemistry B*, 2006, **110**, 8576-8581, doi: 10.1021/jp057478f.
[37] D. Duhovny, R. Nussinov, H. J. Wolfson, Efficient unbound docking of rigid molecules, *Algorithms in Bioinformatic*, 2002, **2452**, 1-15, doi: 10.1007/3-540-45784-4_14.
[38] J. Liu, J. feng Lu, J. Kan, X. yuan Wen, C. hai Jin, Synthesis, characterization and in vitro anti-diabetic activity of catechin grafted inulin, *International Journal of Biological Macromolecules*, 2014, **64**, 76-83, doi: 10.1016/j.ijbiomac.2013.11.028.
[39] L. Jiang, J. Yang, Q. Wang, L. Ren, J. Zhou, Physicochemical properties of catechin/β-cyclodextrin inclusion complex obtained via coprecipitation, *CyTA -Journal of Food*, 2019, **17**, 544-551, doi: 10.1080/19476337.2019.1612948.
[40] W. Zhang, X. Li, T. Yu, L. Yuan, G. Rao, D. Li, C. Mu,

Preparation, physicochemical characterization and release behavior of the inclusion complex of trans-anethole and β-cyclodextrin, *Food Research International*, 2015, **74**, 55-62, doi: 10.1016/j.foodres.2015.04.029.
[41] S. Gao, C. Bie, Q. Ji, H. Ling, C. Li, Y. Fu, L. Zhao, F. Ye, Preparation and characterization of cyanazine-hydroxypropyl-beta-cyclodextrin inclusion complex, *RSC Advances*, 2019, **9**, 26109-26115, doi: 10.1039/c9ra04448e.
[42] D. Han, Z. Han, L. Liu, Y. Wang, S. Xin, H. Zhang, Z. Yu, Solubility Enhancement of Myricetin by Inclusion Complexation with Heptakis-O-(2-Hydroxypropyl)-β-Cyclodextrin: A Joint Experimental and Theoretical Study, *International Journal of Molecular Sciences*, 2020, **21**, 1-11, doi: 10.3390/ijms21030766.
[43] Y. Xu, C. Liu, Q. Wang, X. Zhang, L. Yang, X. Yang. Characterization and antimicrobial activity of rubropunctatin/β-cyclodextrin inclusion complex, *RSC Advances*, 2019, **9**, 7805–7812. doi: 10.1039/C9RA00379G.
[44] S. Ho, Y. Y. Thoo, D. J. Young, L. F. Siow, Inclusion complexation of catechin by β-cyclodextrins: Characterization and storage stability, *LWT*, 2017, **86**, 555-565, doi: 10.1016/j.lwt.2017.08.041.
[45] R. Sharma, M. Goyal, G. Rath. Cyclodextrin-based inclusion complexes: Applications in drug delivery, *Frontiers in Chemistry*, 2023, **11**, 1053446. doi: 10.3389/fchem.2023.1053446
[46] U. G. Spizzirri, G. Carullo, L. De Cicco, A. Crispini, F. Scarpelli, D. Restuccia, F. Aiello, Synthesis and characterization of a (+)-catechin and L-(+)-ascorbic acid cocrystal as a new functional ingredient for tea drinks, *Heliyon*, 2019, **5**, 1-12, doi: 10.1016/j.heliyon. 2019.e02291.
[47] K. Krishnaswamy, V. Orsat, K. Thangavel, Synthesis and characterization of nano-encapsulated catechin by molecular inclusion with beta-cyclodextrin, *Journal of Food Engineering*, 2012, **111**, 255-264, doi: 10.1016/j.jfoodeng.2012.02.024.
[48] T. Loftsson, M. E. Brewster. Pharmaceutical applications of cyclodextrins: Basic science and product development, *Journal of Pharmacy and Pharmacology*, 2010, **62**, 1607–1621. doi: 10.1111/j.2042-7158.2010. 01030.x
[49] J. Szejtli, Introduction and general overview of cyclodextrin chemistry, *Chemical Reviews*, 1998, **98**, 1743–1754. doi: 10.1021/cr970022c
[50] J. Wang, Y. Cao, B. Sun, C. Wang, Physicochemical and release characterisation of garlic oil-β-cyclodextrin inclusion complexes, *Food Chemistry*, 2011, **127**, 1680-1685, doi: 10.1016/j.foodchem.2011.02.036.
[51] R. Zhao, C. Sandström, H. Zhang, T. Tan. Molecular Dynamics Simulations of the Interaction between a Peptide and a Membrane: A Study of the Antimicrobial Peptide LL-37, *Molecules*, 2016, **4**, 372. doi: 10.3390/molecules21040372.
[52] L. Chaput, L. Mouawad, J. Efficient conformational sampling and weak scoring in docking programs? Strategy of the wisdom of crowds, *ChemInform*, 2017, **9**, 1-18, doi: 10.1186/s13321-017-0227-x.
[53] T. Charoenwongpaiboon, A. Oo, S. Nasoontorn, T. Rungrotmongkol, S. Kanokmedhakul, P. Mahalapbutr, Aurisin A Complexed with 2,6-Di-O-methyl-β-cyclodextrin Enhances Aqueous Solubility, Thermal Stability, and Antiproliferative Activity against Lung Cancer Cells, *International Journal of Molecular Sciences*, 2022, **23**, 1-16, doi: 10.3390/ijms23179776.
[54] C. Deng, C. Cao, Y. Zhang, J. Hu, Y. Gong, M. Zheng, Y. Zhou, Formation and stabilization mechanism of β-cyclodextrin inclusion complex with C10 aroma molecules, *Food Hydrocolloids*, 2022, **123**, 1-12, doi: 10.1016/j.foodhyd.2021.107013.
[55] K. Jitapunkul, P. Toochinda, L. Lawtrakul, Molecular dynamic simulation analysis on the inclusion complexation of plumbagin with β-cyclodextrin derivatives in aqueous solution, *Molecules*, 2021, **26**, 1-18, doi: 10.3390/molecules26226784.
[56] L. I. Matienko, E. M. Mil, A. A. Albantova, A. N. Assessing the Performance of MM/PBSA, MM/GBSA, and QM-MM/GBSA Approaches on Protein/Carbohydrate Complexes: Effect of Implicit Solvent Models, QM Methods, and Entropic Contributions, *International Journal of Molecular Sciences*, 2023, **24**, 1-18, doi: 10.3390/ijms242316874.
[57] E. Wang, H. Sun, J. Wang, Z. Wang, H. Liu, J. Z. H. Zhang, T. Hou, End-Point Binding Free Energy Calculation with MM/PBSA and MM/GBSA: Strategies and Applications in Drug Design, *Chemical Reviews*, 2019, **119**, 9478-9508, doi: 10.1021/acs.chemrev.9b00055.
[58] W. M. Menzer, C. Li, W. Sun, B. Xie, D. D. L. Minh, Simple Entropy Terms for End-Point Binding Free Energy Calculations, *Journal of Chemical Theory and Computation*, 2018, **14**, 6035-6049, doi: 10.1021/acs.jctc.8b00418.
[59] S. Fulda, K. M. Debatin, Extrinsic versus intrinsic apoptosis pathways in anticancer chemotherapy, *Oncogene*, 2006, **25**, 4798-4811. doi: 10.1038/sj.onc.1209608
[60] M. M. Gottesman, T. Fojo, S. E. Bates, S. E. Multidrug resistance in cancer: Role of ATP–dependent transporters, *Nature Reviews Cancer*, 2002, **2**, 48–58. doi: 10.1038/nrc706
[61] E. J. Calabrese, Hormesis: Why it is important to toxicology and toxicologists, *Environmental Toxicology and Chemistry*, 2008, **27**, 1451-1474. doi: 10.1897/07-541.1
[62] O. A. Peña-Morán, M. L. Villarreal, L. Álvarez-Berber, A. Meneses-Acosta, V. Rodríguez-López, Cytotoxicity, post-treatment recovery, and selectivity analysis of naturally occurring podophyllotoxins from Bursera fagaroides var. fagaroides on breast cancer cell lines, *Molecules*, 2016, **21**, 1-15, doi: 10.3390/molecules21081013.